Growth and structure of ultrathin vanadium oxide layers on Pd(111)

S. Surnev, L. Vitali, M. G. Ramsey, and F. P. Netzer
Institut für Experimentalphysik, Karl-Franzens-Universität Graz, A-8010 Graz, Austria

G. Kresse and J. Hafner
Institut für Materialphysik, Universität Wien, A-1090 Wien, Austria
(Received 22 November 1999)

The growth of thin vanadium oxide films on Pd(111) prepared by reactive evaporation of vanadium in an oxygen atmosphere has been studied by scanning tunneling microscopy (STM), low-energy electron diffraction (LEED), and *ab initio* density-functional-theory (DFT) calculations. Two-dimensional (2D) oxide growth is observed at coverages below one-half of a monolayer (ML), displaying both random island and step-flow growth modes. Above the critical coverage of 0.5 ML, three-dimensional oxide island growth is initiated. The morphology of the low-coverage 2D oxide phase depends strongly on the oxide preparation conditions, as a result of the varying balance of the mobilities of adspecies on the substrate terraces and at the edges of the growing oxide islands. Under typical V oxide evaporation conditions of $p(O_2)=2\times10^{-7}$ mbar, T(substrate) $=523$ K, the 2D oxide film exhibits a porous fractal-type network structure with atomic-scale ordered branches, showing a $p(2\times2)$ honeycomb structure. *Ab initio* DFT total-energy calculations reveal that a surface oxide model with a formal V_2O_3 stoichiometry is energetically the most stable configuration. The simulated STM images show a (2×2) honeycomb structure in agreement with experimental observation. This surface-V_2O_3 layer is very different from bulk V_2O_3 and represents an interface stabilized oxide structure. The V oxide layers decompose on annealing above 673 K and 2D island structures of V/Pd surface alloy and metallic V are then formed on the Pd(111) surface.

I. INTRODUCTION

Oxide-on-metal epitaxy is an interesting area of interface science and of technological potential because of the importance of ultrathin oxide films in many areas of advanced technology. In spite of their practical relevance, the detailed understanding of the growth processes of thin oxide layers on metal surfaces on a microscopic level is still poorly developed. Vanadium oxides are an interesting class of materials, in which V can occur in various oxidation states ranging from V^{2+} (VO) to V^{5+} (V_2O_5). They exhibit a number of intriguing solid-state properties, such as metal-insulator transitions and unusual magnetic properties.[1] From the viewpoint of surface chemistry, they constitute well-known catalysts for the oxidation of hydrocarbons and of SO_2 to SO_3, for the removal of NO_x by selective reduction with NH_3, and for other reactions.[2] Thin layers of V oxide on metal surfaces have been prepared on Au(111),[3] Cu(100),[4] Ni(110),[5,6] and Rh(111) substrate surfaces.[7] These studies have concentrated on questions concerning the oxide preparation and surface chemistry related aspects. The preparation and reactivity of ordered V_2O_3 films with the corundum structure, obtained by layer-by-layer oxidation of vanadium, were reported first on the Au(111) surface.[3] In a series of papers, Kishi *et al.* have studied the growth and structure of thin V oxide layers on Cu(100) (Refs. 4 and 5) and Ni(110) surface,[6] and have found the formation of a V_2O_3-like oxide phase after room-temperature oxidation of thin vanadium overlayers on Cu(100).[4] Further oxidation of the vanadium to V^{5+} has been detected in the presence of sodium.[4] A growth of VO(111)-like structures was observed when V layers were oxidized at 250 °C on Cu(100) (Ref. 5) and Ni(110) surfaces.[6] The growth of VO_x islands on Rh(111) has been studied by conventional x-ray photoelectron spectroscopy (XPS) as a model system for vanadia-promoted Rh catalysts by Hartmann and Knözinger.[7]

Recently, we performed a high-resolution electron spectroscopy study with use of synchrotron radiation on the nature and stability of V oxides on Pd(111) as a function of the oxide coverage and temperature.[8] This study was motivated by a search for a catalytic model system, which can mimic the so-called ''strong metal-support interaction'' (SMSI) effect. The V oxides have been prepared by reactive evaporation of vanadium in an oxygen atmosphere from submonolayer to 15-monolayer (ML) coverages. It was found that the oxide stoichiometry is coverage dependent: VO/VO_2-like at low coverages and V_2O_3 for thicker oxide layers. The V_2O_3 phase grows epitaxially on the Pd(111) surface in the form of small three-dimensional (3D) islands as revealed by low-energy electron-diffraction (LEED) and scanning tunneling microscopy (STM).[8]

Here we report a more detailed combined experimental and theoretical study on the growth and structure of ultrathin V-oxide films on Pd(111). The growth processes and the evolution of surface structures have been investigated experimentally by STM and LEED, whereas the surface structures of thin layers of V oxides on Pd(111) have been modeled theoretically by *ab initio* density-functional theory (DFT) total-energy calculations. In this paper we focus on the low coverage regime, below the critical coverage of one-half monolayer, which marks the onset of the population of the second oxide layer. The various ordered surface structures which are obtained at around 1-ML nominal oxide coverage

will be described and discussed in a forthcoming companion paper.[9]

We observe a morphology of the V-oxide low coverage phases, which depends strongly on the details of the conditions of oxide preparation, namely the pressure of oxygen and the substrate temperature during the reactive evaporation process of vanadium. The growth mode includes step-flow and random island formation processes, and the balance of the adatom mobilities at the substrate terraces and along the edge boundaries of the growing oxide nuclei are shown to play critical roles in determining the oxide island shapes. Interface-stabilized 2D oxide structures have been observed in atomically resolved STM images, which are analyzed with the help of *ab initio* total-energy DFT calculations.

II. EXPERIMENT AND COMPUTATION

A. Experimental procedure

The experiments were conducted in two custom-designed ultrahigh-vacuum (UHV) systems, operating both at base pressures $<2\times10^{-10}$ mbar. They are equipped with crystal cleaning, evaporation, low-energy electron diffraction (LEED), Auger electron spectroscopy (AES), and STM facilities. In the first system, which has been described elsewhere,[10] an Omicron micro-STM operated at room temperature has been used. In the second system, STM experiments were performed with a variable temperature STM (Oxford Instruments), which was operated also at room temperature in this particular study. Here, the sample with dimensions $5\times5\times1$ mm^3 is mounted in a Mo holder, which can be transferred with a manipulator between the microscope and different positions in the chamber for surface preparation (sputtering, evaporation) and characterization (LEED, AES). The sample can be heated up to 1500 K by electron bombardment from the back side and the temperature is measured with a NiCr-Ni thermocouple mounted on the sample holder. The microscope stage allows sample heating by radiation from a W filament (up to 1000 K) or cooling (down to $<$50 K) by contact to a liquid He cryostat, while tunneling. The whole UHV chamber hangs on springs ($\sim$180 cm long in the extended state) from the ceiling of the laboratory. This ensures a low resonant frequency of below 0.5 Hz for the whole system, leading to an efficient vibration isolation.

Clean Pd(111) crystal surfaces were prepared by 1-keV argon-ion sputtering followed by annealing to 1100 K. Two different Pd(111) crystals, one for each system described above, were employed. The cleanliness of the Pd surfaces were checked by AES and LEED. STM showed clean and flat terraces, separated by straight monatomic steps. The average terrace widths ranged from 100 to 3000 Å, with the Pd(111) crystal of the second system exhibiting the higher step density. Vanadium (purity 99.8%, Goodfellow Metals) was deposited from a well degassed water-cooled electron beam evaporator (Omicron EFM3). The V deposition rate was monitored by a quartz crystal microbalance and checked with STM by measuring the surface area of two-dimensional (2D) V-metal islands grown at submonolayer coverages onto Pd(111) at 400 K (at higher temperatures, diffusion of V into the Pd bulk has been observed).

Clean vanadium-oxide layers were prepared using the procedure established in a previous study,[8] which consists of the evaporation of V onto the clean Pd(111) surface at 523 K in an oxygen atmosphere of 2×10^{-7} mbar. Since the true vanadium-oxide coverage is strongly dependent on the stoichiometry and morphology of the oxide phase, it will be given in monolayer equivalents (MLE). Accordingly, 1-MLE V-oxide film corresponds to a V content of 1 ML of V on the Pd(111) surface (i.e., 1.52×10^{15} atoms per cm^2). The V deposition rate was varied between 0.1- and 0.4-ML min^{-1}, depending on the desired oxide thickness. Postannealing of the V-oxide layers has been performed in the temperature range 573–773 K in UHV.

All STM images were recorded in a constant current mode. Electrochemically etched tungsten tips were used, cleaned *in situ* by electron bombardment. The sample bias voltage was set between -2 and $+2$ V, and the tunneling current between 0.05 and 2 nA. During the measurement of the oxide surfaces, frequent tip changes were observed in the STM images, probably due to a transfer of atoms from the surface to the tip.

B. Computation

Our first-principles calculations are based on density-functional theory (see, e.g., Ref. 11) employing a plane-wave basis set.[12] To solve the Kohn-Sham equations, we use the Vienna *ab initio* simulation package (VASP),[13,14] which calculates the Kohn-Sham ground state via an iterative unconstrained band-by-band matrix diagonalization scheme and an optimized charge-density mixing. The electron-ion interaction is described by the projector augmented wave (PAW) method as proposed by Blöchl.[15] Compared to conventional pseudopotentials, this method has the advantage that the exact shape of the valence wave functions is taken into account, and this in turn can improve the description of transition metals.[16] A pseudization radius of 1.25 and 1.2 Å is used for Pd and V, respectively. The $3p$ states of V are treated as valence states to guarantee a good transferability of the V potential. For oxygen, pseudization radii of 0.8 and 0.95 Å are used for the s and p states. All calculations are performed at an energy cutoff of 250 eV, resulting in an accurate description of the Pd bulk, Pd surface, and bulk vanadium oxides. These results will be presented elsewhere.[17] In all calculations, we use the generalized gradient corrections (GGA) of Perdew and Wang,[18] commonly referred to as PW91. The slab supercell approach with periodic boundaries is employed to model the surface, and the Brillouin-zone (BZ) sampling is based on the Monkhorst-Pack technique.[19] For the calculation of the fractional occupancies, a broadening approach, proposed by Methfessel and Paxton,[20] is used with $N=1$ and $\sigma=0.2$ eV. The relaxation of the ionic positions into the ground-state geometry is performed with a quasi-Newton scheme.

In the present work, the Pd surface is modeled by four Pd layers of which two layers are allowed to relax. To sample the band structure, a grid corresponding to $8\times8\times1$ k points in the primitive surface cell is chosen. With this setup, we estimate that typical errors in the calculation of the adsorption energy are 20 meV per adatom. This was confirmed by performing calculations for selected configurations with six-

layer-thick slabs and a denser *k*-point grid. The adsorption energies changed by typically 15 meV/adatom. In total, more than 20 structures were considered, but here we will limit our discussion to the three most stable structures with the formal compositions V_2O_3, VO, and V_3O_2. For these three structures, constant current STM topographs are simulated by calculating the local energy resolved density of states $\rho(\mathbf{r},\varepsilon)$ in the vacuum. We evaluate isosurfaces of constant charge density $\rho(\mathbf{r},\varepsilon)=C$, and determine the corrugation of these isosurfaces. Typically the isosurfaces are determined at an average distance of 3 Å from the core of the outermost atoms. Although this is a much simplified approach, which is not expected to give quantitative agreement with the experiment, we believe that qualitative features are well reproduced by this simple method. Finally, selected vibrational frequencies have been calculated by diagonalization of the dynamical matrix of the V-O subsystem; the Pd substrate was kept rigid in those calculations.

III. RESULTS AND DISCUSSION

A. V-oxide growth morphology ($0<\Theta\leqslant 2$ MLE)

Figure 1 presents large-scale STM images of consecutive vanadium-oxide growth stages on Pd(111) prepared at the typical evaporation conditions: T(substrate temperature) $=523$ K, $p(O_2)=2\times10^{-7}$ mbar. Note that the STM images have not been obtained from the same area of the Pd(111) crystals, thus the step densities vary from image to image. At low coverages ($\Theta\leqslant 0.25$ MLE), the vanadium-oxide growth is observed to follow both island and step-flow growth modes: the oxide nucleates along the step edges and as 2D islands on the terraces (marked 1 in Fig. 1). On small terraces the oxide phase decorates preferentially the step edges on the lower terrace [see Fig. 1(c)]. Similar growth behavior has been recently reported by Weiss and Ritter[21] for thin FeO layers on Pt(111), which indicates a preferred downward step diffusion of the oxide. On the larger terraces 2D islands also form, which are not compact but exhibit a complex porous network structure, which will be shown in more detail later on. Some small bright clusters are visible on the Pd terraces and on the oxide islands, which cause frequently tip instabilities. These clusters decorate also the upper step edges. Since AES indicates clean surface conditions, these features are probably disordered clusters of V oxide. Increasing the oxide coverage leads to an enlargement of the 2D islands and of the oxide phase at the steps [Fig. 1(b)], and then to the coalescence into a 2D porous overlayer at around 0.4 ML [Fig. 1(c)], which does not completely cover the entire Pd(111) surface. At a critical coverage of half a monolayer [Fig. 1(d)], the second oxide layer becomes populated. In Fig. 1(d) free Pd areas, first-layer oxide (marked 1) and second-layer oxide (marked 2), can be distinguished on the basis of higher resolution images. The growth of small third-layer areas is then observed on top of the second layer [marked 3, Figs. 1(e) and 1(f)]. Hence, the coverage of 0.5 MLE marks the transition from two- to three-dimensional (3D) oxide growth. Note that bare Pd patches (dark areas) coexist with the oxide islands up to $\leqslant 1$ MLE. At 1 MLE [Fig. 1(e)] the growth of the first oxide layer is completed and the surface is heterogeneous, consisting of first-, second-, and third-layer oxide islands. Higher resolution images (not shown here) reveal that mainly two types of 3D islands exist at 1 MLE with different surface structures. At an oxide coverage of 2 MLE [Fig. 1(f)] the Pd(111) surface is fully covered by 3D islands, with lateral dimensions between 50 and 200 Å. LEED from this surface shows a $(\sqrt{3}\times\sqrt{3})R30°$ pattern, and high-resolution STM images from the top facets of the islands (not shown) reveal a hexagonal surface structure with an atomic periodicity of 5.0 ± 0.2 Å, in agreement with the LEED pattern. Very similar results have been obtained in our previous study for a V-oxide thickness of 5 MLE, where the 3D islands have been attributed to epitaxially grown V_2O_3 crystallites with corundum structure, terminated by the (0001) face parallel to the Pd(111) surface.[8]

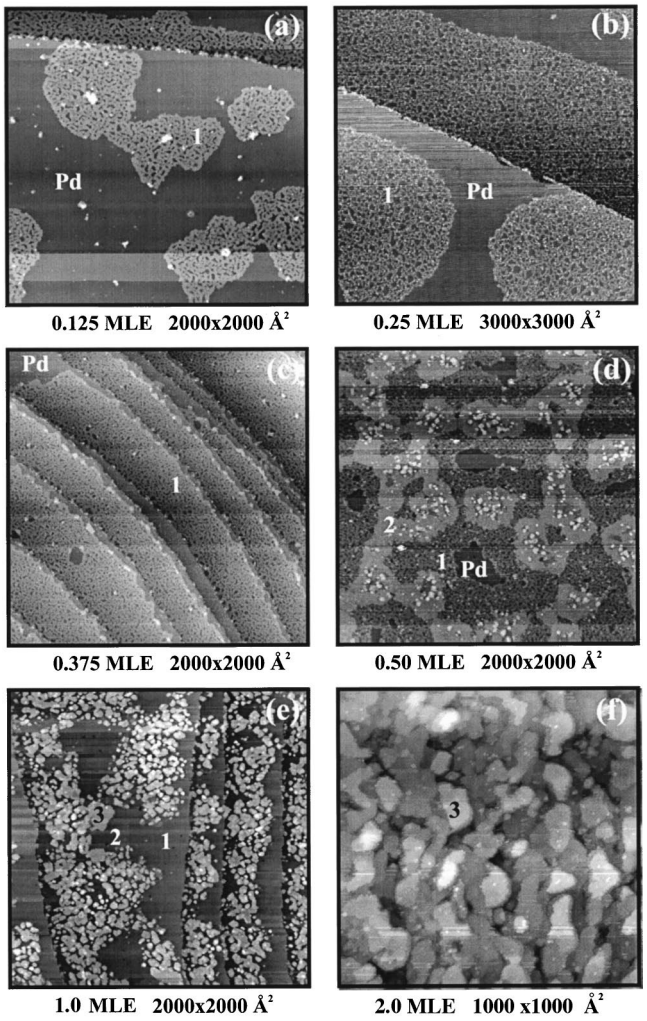

FIG. 1. Large-scale STM images of V-oxide films grown on Pd(111) at $T=523$ K and an oxygen pressure of 2×10^{-7} mbar. The indications ''1'' and ''2'' refer to the first and second oxide layers, respectively, and ''3'' to the 3D oxide islands.

A more detailed study on the morphology and structure of the different 3D V-oxide phases, which are observed beyond the critical coverage of 0.5 MLE, will be presented in a forthcoming paper.[9] Here we will concentrate on the morphology and structure of V-oxide films in the submonolayer coverage range $0<\Theta<0.5$ MLE, i.e., up to the critical coverage of the onset of growth of the second layer. The oxide coverage of 0.25 MLE has been chosen as representative of the behavior of the adlayer in this regime and therefore all

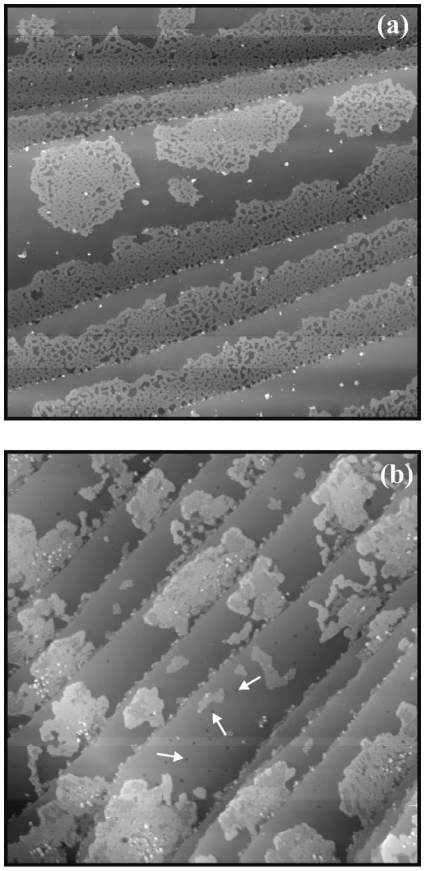

FIG. 2. 3000×3000-Å^2 STM images of 0.25-MLE V-oxide films grown on Pd(111) at $T=523$ K and oxygen pressures of (a) 1×10^{-6} mbar and (b) 5×10^{-8} mbar. Arrows indicate pit holes, as mentioned in the text.

the experimental data presented in the following will refer to this particular coverage. The effects of the evaporation conditions and the post-annealing in UHV on the oxide morphologies will be considered, and an analysis based on the STM data and on first-principle calculations of the atomic structure of the oxide layer will be presented.

B. Oxygen pressure and temperature dependence of the V-oxide growth morphology

The oxide film evaporation parameters, such as ambient oxygen pressure, substrate temperature, and metal deposition rate are of critical importance for the oxide stoichiometry, morphology, and structure. In this section the effects of two of them, the oxygen pressure and the substrate temperature, on the growth morphology of thin vanadium-oxide films is investigated. Figure 2 displays large-scale STM images after evaporation of 0.25 MLE V onto the Pd(111) surface held at 523 K for oxygen pressures of 1×10^{-6} mbar [Fig. 2(a)] and 5×10^{-8} mbar [Fig. 2(b)]. As seen in Fig. 2(a), the morphology of the V-oxide layers formed at 1×10^{-6} mbar O_2 does not differ substantially from that obtained at 2×10^{-7} mbar O_2 [see Figs. 1(b) and 3(c)]: it consists of porous 2D oxide islands on the terraces and a step-edge decorating 2D layer. The apparent height of these structures [relative to the Pd(111) surface] is rather low, about 1.1 ± 0.1 Å. For comparison, the height of metallic vanadium islands grown on the Pd(111) surface at 400 K has been measured to be ≈2.3 Å. No change of the oxide island height has been observed, if the bias voltage was varied between −2 and +2 V. Similar small apparent heights have also been observed for NiO and FeO islands grown in the submonolayer range on Au(111) (Ref. 22) and Pt(111) (Ref. 23) substrates, respectively. It has been suggested that they reflect the differences in the electronic structure of the metallic substrate and oxide islands.[22] At lower oxygen pressures [Fig. 2(b)] more compact, less branched 2D islands grow on the Pd(111) surface and the step edges are no longer decorated. The maximum height of the islands of 2.3 ± 0.1 Å is very close to that of metallic V islands. This suggests that the oxidation of vanadium at an oxygen pressure of 5×10^{-8} mbar is incomplete. In Fig. 2(b), dark holes due to pitting are recognized on the bare Pd terraces, which are possibly due to the diffusion of V into the Pd bulk, as discussed later.

Figure 3 illustrates the effect of the substrate temperature on the oxide growth morphology for 0.25 MLE V oxide evaporated onto Pd(111) in 2×10^{-7} mbar O_2 atmosphere. At substrate temperatures <523 K [Figs. 3(a) and 3(b)] the oxide layers exhibit similar morphologies, with an irregular meandering network of 2D island structures covering the entire surface. These islands appear to be internally compact and no preferred decoration of the step edges is observed. At 453 K [Fig. 3(a)] numerous small bright features are visible on top of the V-oxide islands, presumably due to disordered oxide clusters. For oxide films evaporated at 493 K [Fig. 3(b)] the islands develop sharper contours in the STM image and no clusters are detected on their top surface. At 523 K [Fig. 3(c)] the oxide layer changes the morphology, displaying the porous network structure as mentioned above. Note that the oxide layer is now also decorating the lower step edges, indicating the onset of the step-flow mechanism at that temperature. The observed temperature dependence of the oxide growth morphology may be associated with a change of balance between the mobility of V and O adspecies on the Pd terraces and on the growing edge boundaries of the oxide nuclei. At 523 K, the terrace mobility appears to be increased over that at the lower substrate temperatures, but the low edge mobility leads to the fractal-type growth behavior yielding the porous oxide structures as observed [Fig. 3(c)].

C. Effect of the annealing on the V-oxide morphology and structure

Figure 4 shows large-scale (left) and atomic resolution (right) STM images of 0.25-MLE vanadium-oxide films as evaporated and after annealing in UHV to temperatures in the range 573–773 K. As already mentioned, the oxide film after the evaporation [$T=523$ K, $p(O_2)=2\times10^{-7}$ mbar] exhibits an irregular porous network morphology with many internal holes [Fig. 4(a)]. The network is, however, well ordered at the atomic scale as revealed by the high-resolution STM image. The branches, which enclose bare Pd areas within the network, display a $p(2\times2)$ honeycomb structure [see inset of Fig. 4(a), right panel]. The boundaries of the network branches are ragged, but appear to be made up mostly by complete honeycomb unit cells. The network re-

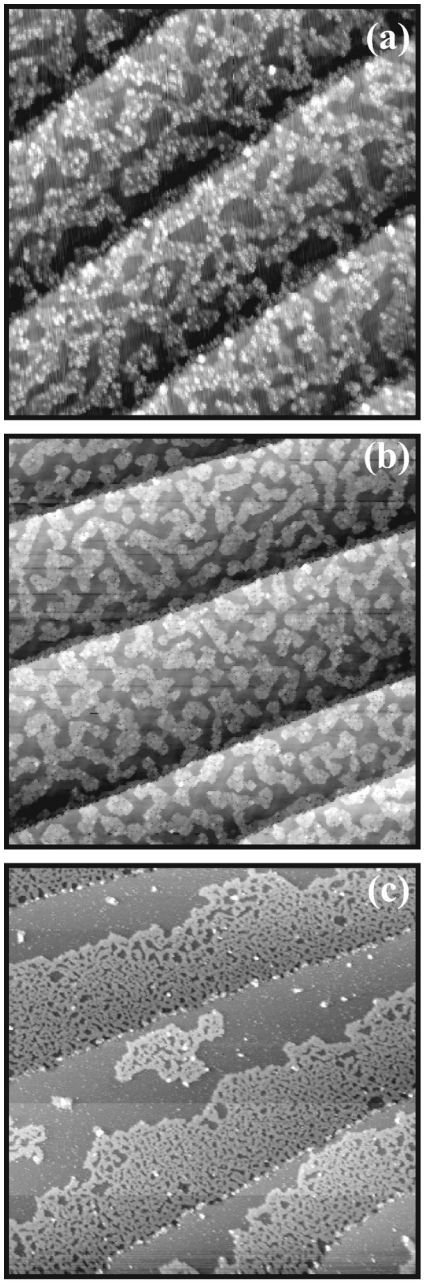

FIG. 3. 3000×3000-Å^2 STM images of 0.25-MLE V-oxide films grown on Pd(111) at an oxygen pressure of 2×10^{-7} mbar and at (a) $T=453$ K, (b) $T=473$ K, and (c) 523 K.

sembles in some way the random fractal patterns, which are observed during the growth of submonolayer metal films on (111) fcc metal surfaces.[24,25] In general, the fractal geometry is associated with a kinetically- or impurity-hindered diffusion of adspecies along the edges of growing islands (''hit and stick'' mechanism). In the present case, surface oxygen, present during reactive evaporation, could play the role of an impurity, which hinders the diffusion along the edges of small aggregates and prevents the formation of more compact oxide structures.

Immediately after the oxide evaporation, LEED shows a $p(4\times4)$ pattern, which, however, transforms within a few minutes into a $p(2\times2)$ pattern at room temperature. We found that this transformation occurs independently of whether the sample is illuminated with slow electrons in LEED or not, which suggests that this $p(4\times4)$ structure is only metastable. The $p(2\times2)$ LEED pattern is not very sharp at this point, which is consistent with some disorder and the relatively small area of the (2×2) oxide phase. It is interesting to notice that oxygen dosed in similar amounts as during the evaporation ($\sim$40 L) on clean Pd(111) at 523-K temperature produces also a weak $p(2\times2)$ LEED pattern, due to the presence of ordered islands of chemisorbed oxygen on the Pd surface.[26] For the V-oxide covered Pd(111) surface, however, there is an indication that the $p(2\times2)$ LEED structure is related mainly to the oxide phase: (i) atomic ordering with $p(2\times2)$ periodicity could only be revealed on the oxide islands and not on the bare Pd areas in the STM images; (ii) in view of the much higher reactivity of V towards O as compared with Pd, most of the oxygen bounds preferably to V, as indicated by the first-principle DFT calculations.[27]

Figure 4(b) shows that annealing the vanadium-oxide film to 573–623 K for 3 min leads to pronounced changes in the oxide morphology. The initial porous network structure is now replaced by more compact 2D islands. This may be related with the removal of the excess oxygen from the surface, which tends to migrate into the Pd, bulk at such annealing temperatures.[26] The high-resolution image in Fig. 4(b) (right panel) demonstrates that significant improvement of the atomic order within the oxide islands occurs upon annealing. Here, three (2×2) domains are seen, which are separated by domain boundaries (arrows). On top of the (2×2) layer some bright protrusions are clearly visible, which are due to single atoms from the second layer, possibly O or V adatoms. STM images, taken at reduced positive bias, provide additional information on the atomic structure of the (2×2) oxide phase. A high-resolution image of the oxide island, taken at a bias of $+100$ mV, is presented in the inset on the right-hand side of Fig. 4(b). It shows the (2×2) honeycomb lattice, with 5.5 ± 0.2 Å separations, which is twice the Pd-Pd distance at the (111) surface (2.75 Å). This is in accord with the observed $p(2\times2)$ pattern in LEED, which has become much sharper after the annealing step to 623 K. Further details of the (2×2) honeycomb structure will be discussed in the next section.

Figure 4(c) shows that annealing of the 0.25 MLE V-oxide/Pd(111) surface to 673 K results in a partial replacement of the (2×2) oxide phase by a new ordered surface structure with an apparent height of 1.6 ± 0.1 Å, relative to the Pd(111) surface. A closer look at this new phase shows an interesting bias dependence. At a bias voltage of $+2$ V [see inset in Fig. 4(c), left panel] it is imaged as a hexagonal pattern. The atomic-resolution STM image, taken at $+0.1$ V [right-hand side of Fig. 4(c)], displays a so-called ''wagon wheel'' network coexisting with the honeycomb (2×2) superstructure and bare Pd areas. The ''wagon wheel'' network has an apparent corrugation of 1.2 ± 0.1 Å, smaller than that of the hexagonal pattern. Both hexagonal and ''wagon wheel'' superstructures exhibit a large hexagonal unit cell with the same periodicity of 21.8 ± 0.2 Å, which is rotated by $19°\pm1°$ with respect to the (2×2) unit cell of the oxide layer [or the Pd(111) surface]. It can be described by $(\sqrt{63}\times\sqrt{63})R19.1°$ or by a $\begin{pmatrix}9&4\\-4&5\end{pmatrix}$ superstructure cell, using the Wood or matrix notation, respectively. Very similar structures have been recently reported by Zhang *et al.*[28] for Cr

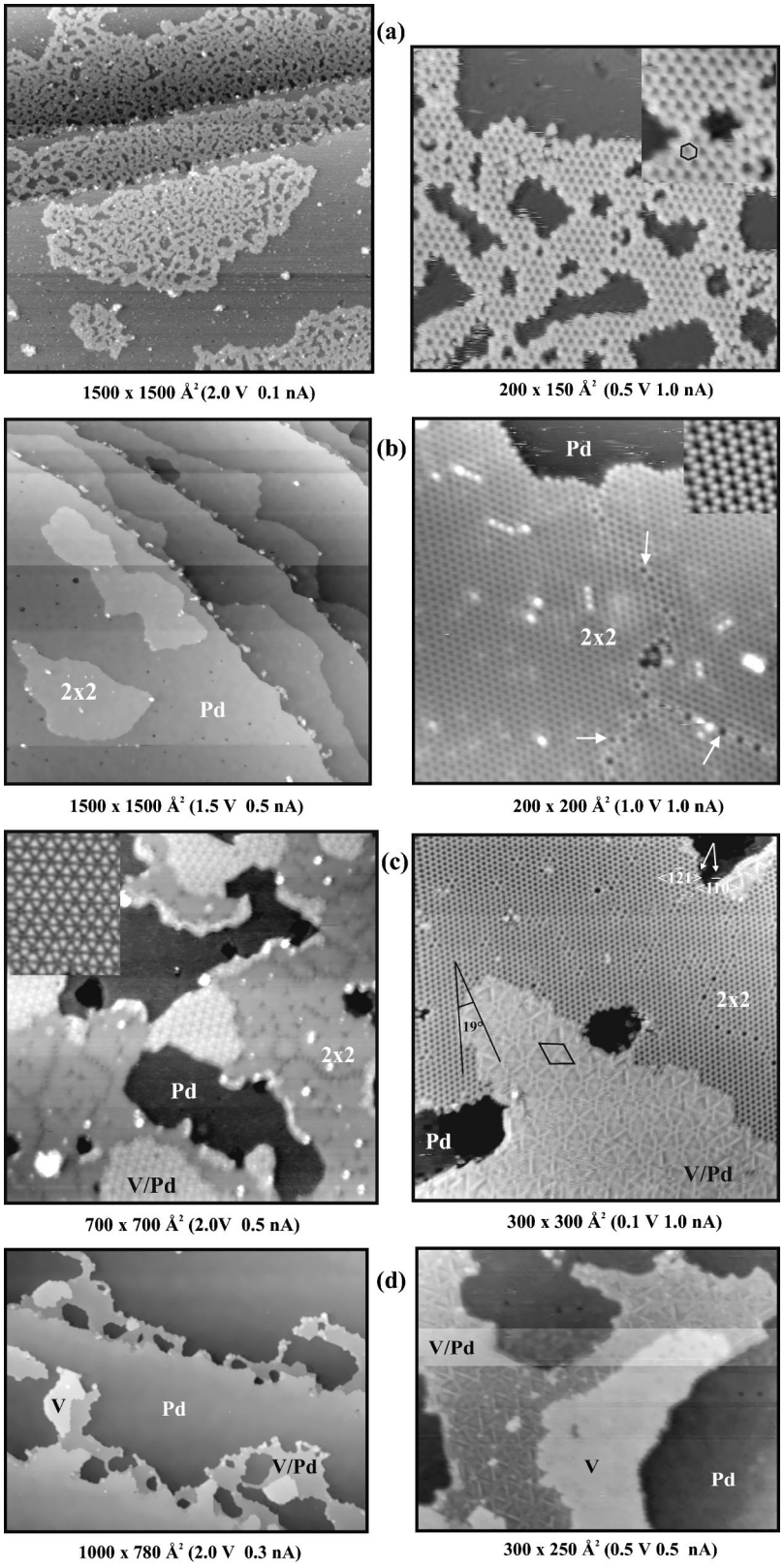

FIG. 4. Large-scale (left) and atomic resolution (right) STM images of 0.25-MLE V-oxide films grown on Pd(111) at $p(O_2)=2\times10^{-7}$ mbar, $T=523$ K, and post-annealed in vacuum. (a) As-deposited (inset: 44×44-Å^2 STM image, 0.5 V, 1.0 nA); (b) annealed to 623 K (inset: 31×31-Å^2 STM image, 100 mV, 1.0 nA); (c) annealed to 673 K (inset: 150×190-Å^2 STM image, 2.0 V, 0.6 nA); (d) annealed to 773 K.

overlayers on Pt(111) annealed to 800 K, which display in general similar bias dependence. They have been attributed to the formation of an ordered Cr/Pt surface alloy.[28] It is likely that such an alloy formation also takes place between the V and Pd after annealing to 673 K. Our XPS results[8] have demonstrated that annealing of thicker (1.0–2.5 MLE) V-oxide films on Pd(111) to 673 K leads to the appearance of a component in the V $2p_{3/2}$ core-level spectra with a binding energy of 513.6 eV, which has been ascribed to a V/Pd alloy. Therefore, the temperature of 673 K marks the onset of the V-oxide decomposition.

Annealing the 0.25-MLE oxide phase to 773 K leads to a complete decomposition of the vanadium oxide. The STM images [Fig. 4(d)] show that the fraction of the Pd(111) sur-

face covered with 2D islands is significantly reduced. Two types of islands can be distinguished: (i) dendriticlike shapes with an apparent height of 1.2 ± 0.1 Å; (ii) more compact structures with an apparent height of 2.2 ± 0.1 Å. As is evident from the high-resolution image [Fig. 4(d), right panel], the dendritic islands can be ascribed to the V/Pd alloy phase, which displays the characteristic ''wagon wheel'' network structure. The second type of island is attributed to metallic vanadium. This interpretation is based on the height of these islands, which is very close to that measured on metallic V islands on Pd(111) (2.3 Å) and on the V $2p_{3/2}$ XPS spectra. In the latter two spectral components, binding energies of 513.2 and 513.6 eV have been obtained for 1-MLE V-oxide/Pd(111) annealed to 773 K, which have been ascribed to metallic vanadium and the V/Pd alloy, respectively.[8]

The formation of a well-ordered V/Pd surface alloy on heating the V-oxide film to 773 K deserves further comment. This phase was found for the whole oxide coverage range studied, with the formation temperature shifting slightly to higher values at higher coverage. It is interesting to note that such surface alloy structures have not been observed when evaporating metallic V onto Pd(111) and subsequently annealing to 773 K. Under these conditions, only small pits were visible on the Pd terraces after the annealing; the whole V has diffused into the Pd bulk. This behavior is in agreement with the DFT calculations, indicating that V prefers a high coordination with Pd.[27] The stability of the V/Pd surface alloy after oxide decomposition could be explained by the presence of subsurface oxygen on Pd(111), which may hinder the V diffusion into the Pd bulk. This diffusion barrier of subsurface oxygen may be built up by oxygen from the gas phase during the reactive evaporation step of the V-oxide films at 523 K and/or from oxygen liberated during the V-oxide reduction at 773 K. As shown recently, the migration of oxygen into the Pd bulk is a dominant process at elevated temperatures.[26] In the case of metallic V on Pd(111), no diffusion barrier exists which prevents the diffusion of V into the Pd lattice. As a result, no stable surface alloy is formed upon heating.

D. The (2×2) oxide structure

We now examine the atomic structure of the (2×2) oxide phase in more detail. As already presented in Fig. 4(b), well-ordered 2D islands with a (2×2) honeycomb structure can be prepared by annealing thin oxide films up to 623 K in vacuum. Figure 5(a) shows a high-resolution STM image revealing bright maxima, arranged in a honeycomb lattice. Some imperfections can be distinguished on the image, such as defects and adspecies, which create local deformations in the (2×2) layer and domain boundaries. Two line scans are displayed in Fig. 5(b), taken along the white lines *a*-*b* and *c*-*d*, i.e., along the $\langle 1\bar{1}0\rangle$ and $\langle 1\bar{2}1\rangle$ crystal directions, respectively. The line profile in the $\langle 1\bar{1}0\rangle$ direction [*a*-*b*, upper plot of Fig. 5(b)] has an average corrugation of about 0.5 Å and shows maxima (minima) separated by 5.5 ± 0.2 Å, which is twice the distance between the Pd atoms in this direction (2.75 Å). The line scan in the $\langle 1\bar{2}1\rangle$ direction [*c*-*d*, lower plot of Fig. 5(b)], which connects the neighboring features of the honeycomb cell, reveals that there are minor height differences of the order of 70 pm between them. This apparent height difference is almost insensitive to the bias voltage (between +10 mV and +1.0 V), suggesting that it reflects the geometrical structure of the oxide. Atomic resolution could not be obtained at higher bias voltages (>1 V). Images at negative bias voltages, imaging the filled states, were generally of poorer quality and are therefore not presented.

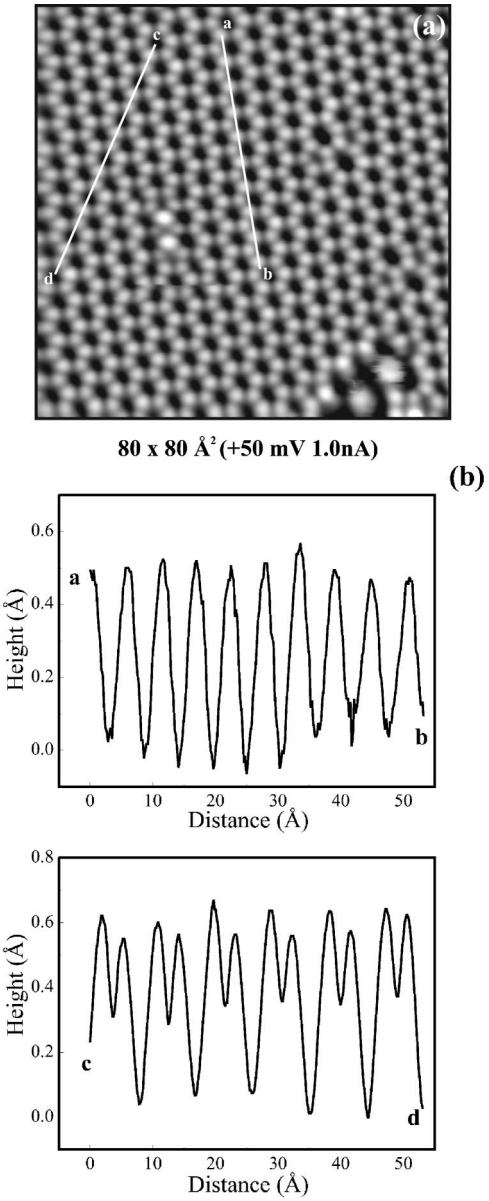

FIG. 5. (a) High-resolution 80×80-Å^2 STM image of the honeycomb $p(2\times2)$ V-oxide surface, prepared after annealing 0.25 MLE, grown at 523 K in 2×10^{-7} mbar oxygen pressure, to 623 K in vacuum; (b) line scans *a*-*b* and *c*-*d*, taken along the $\langle 1\bar{1}0\rangle$ and $\langle 1\bar{2}1\rangle$ crystal directions, respectively.

E. *Ab initio* calculations

In Fig. 6, the three structure models of the (2×2) surface, which have been explored in more detail, are displayed. For a (2×2) reconstruction and a given stoichiometry, each model is energetically the most stable one we could find in an extensive and careful examination of the configuration

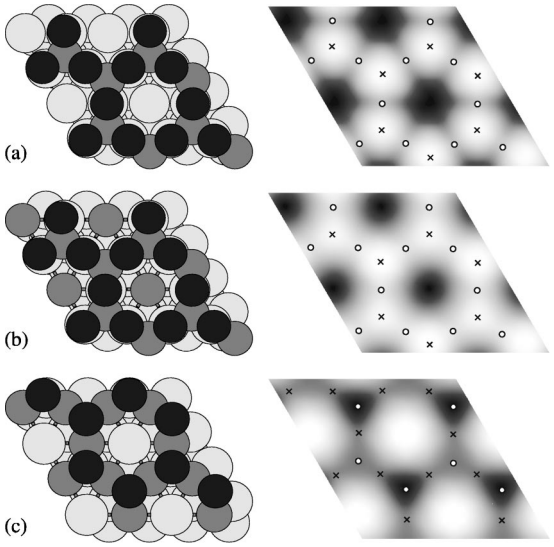

FIG. 6. Surface structure models (left-hand side) considered in the *ab initio* calculations: (a) surface V_2O_3, (b) surface VO, and (c) surface V_3O_2. The simulated empty-state STM images are shown at the right-hand side. Legend: dark circles, O atoms; gray circles, V atoms; and bright circles, Pd atoms. The small crosses and white circles on the simulated STM images indicate the true positions of the V and O atoms, respectively.

space. In the search procedure, initial structural models were either guessed on the basis of chemical intuition, or generated by simulated annealing runs. All initial models were relaxed structurally into the nearest local energy minimum. For a given stoichiometry, different V-O coverages were considered. For the VO stoichiometry, for instance, we performed calculations for (2×2) supercells containing between one and four V and O atoms. In addition, V atoms were allowed to replace Pd atoms in the surface layers, but V atoms in subsurface layers were generally not considered. In the present calculations, only thin layers have been considered, and the V coverage never exceeded 1 ML. This corresponds to the experimental situation under investigation here. More details covering all explored structural models will be presented elsewhere.[17]

It is important to emphasize that we are reasonably confident that no structure of relevance has been overlooked and that the models shown in Fig. 6 represent true structural minima for a (2×2) reconstruction and a given stoichiometry. We will refer to these models as surface V_2O_3, surface VO, and surface V_3O_2, and these must not be mixed up with corresponding bulk structures. The surface-V_2O_3 model [see Fig. 6(a)] is characterized by two V atoms per unit cell adsorbed in the fcc and hcp hollow sites of the Pd(111) surface. The distance of the V atoms from the Pd layer is approximately 2.15 Å. The three oxygen atoms are adsorbed in the V-V bridge sites and are located 0.75 Å above the two V atoms, resulting in a V-O bond length of 1.77 Å. The surface-VO model [Fig. 6(b)] is similar to the surface-V_2O_3 model, but the central surface Pd atom has been replaced by a V atom. The structural parameters for the surface-VO model agree closely with those for the surface-V_2O_3 model. The third stoichiometry considered here is the V_3O_2 case. The structure is characterized by a single layer of three V and one Pd atom per unit cell. All hollow sites with three neighboring V atoms are occupied by O adatoms, which are located about 1 Å above the PdV_3 surface layer. As a result of bond-order conservation, the O-V bond is slightly increased compared to the previous two cases (1.88 Å).

Of the three models explored here, only the surface-V_2O_3 structure is energetically stable. The VO structure decomposes into surface V_2O_3 and surface V_3O_2 with an energy gain of 300 meV per (2×2) surface cell. The V_3O_2 model itself is also unstable, and decomposes into surface V_2O_3 and V in the bulk solution. The energy gain in this case is huge and amounts to 2.6 eV per (2×2) surface cell. However, since migration of V into the bulk is possible only at elevated temperatures, we have included this structure in the analysis. The simulated STM images for the three models are shown on the right-hand side of Fig. 6. For the surface-V_2O_3 and surface-VO models, the simulated images are very similar. This is related to the fact that replacing a Pd surface atom by V in the center of the honeycomb cell hardly affects the electronic structure of the oxide layer. Both simulated STM images are remarkably similar to the experimental one for the (2×2) structure. The simulation indicates that the V atoms are seen as bright maxima, whereas the oxygen atoms cause a significant charge reduction, which is in contrast to the real geometrical height. For surface V_2O_3 the corrugation of the STM image is somewhat larger than in the experiment and amounts to 1.2 Å, whereas for surface VO the simulated corrugation is 0.7 Å. The simulated height of the thin films with respect to the Pd surface is small (1.6 Å), in agreement with the experiment. This is related to the fact that the metallic Pd states extend into the vacuum, whereas the oxide layer effectively screens these states.

Moving to the simulated image of the V_3O_2 structure [Fig. 6(c)], we note already at first sight that the image differs significantly from the experimental results. The oxygen adatoms are again causing charge depletions and charge is also depleted from the neighboring V atoms, probably due to the formation of the oxide. The Pd surface atoms are now visible as bright maxima in the STM simulation. The surface Pd atoms of the clean Pd substrate and the surface Pd atom in the V_3O_2 cell have about the same apparent height in the STM image, whereas the O adatoms have a negative corrugation of -0.6 Å with respect to the clean Pd substrate. We are therefore led to the conclusion that the surface-V_3O_2 model cannot account for the observed STM images, and this agrees with the initial energetic arguments.

The combination of STM simulations and total-energy calculations clearly indicates that the surface-V_2O_3 structure is the best candidate for the experimentally observed (2×2) superstructure. At first sight, this appears to be in contradiction to the oxidation state deduced from XPS core-level shifts of the (2×2) structure, which have suggested a VO stoichiometry.[8] However, it should be kept in mind that a monolayer of V_2O_3 has a completely different structure compared to bulk V_2O_3. In particular, the V atoms are in direct contact with the Pd substrate, which changes the electrostatics and influences the core-level shifts significantly. To obtain some qualitative insight, we have calculated the initial state core-level shifts for the surface-V_2O_3 and surface-VO model, and compared them to the bulk V_2O_3 initial-state core-level energies. The core-level binding energy for the V atoms in contact with the O atoms (surface-V_2O_3 model) is 1

eV smaller than that for bulk V_2O_3, which is in rather good agreement with the observed values in the XPS experiments.[8] For the VO model, the core-level binding energy of the V atom in the surface layer is an additional 1 eV smaller and close to that of a V-Pd surface alloy. This is another argument that seems to rule out the VO as a possible candidate for the (2×2) superstructure, since the experimental synchrotron XPS data have been well fitted with a single core-level component.[8]

Finally, we have calculated the frequency of the Γ-point dipole active phonon mode for the surface-V_2O_3 model. We found a frequency of 68 meV, which is in perfect agreement with high-resolution electron-energy-loss spectroscopy (HREELS) measurements as reported elsewhere.[29] It was also tested whether CO can be adsorbed on the surface-V_2O_3 and surface-V_3O_3 models. Although it was found that CO adsorption is in principle energetically favorable on both surfaces, a large barrier of 400 and 700 meV must be overcome before adsorption can occur. Experimentally, CO adsorption has not been detected on the (2×2) V-oxide surfaces,[8,30] in agreement with the large calculated barriers for CO adsorption.

CONCLUSIONS

The initial growth of thin films of vanadium oxide reactively evaporated onto Pd(111) surfaces has been studied in detail by scanning tunneling microscopy. For low oxide coverages ($\Theta<0.5$ MLE), both island and step-flow 2D growth modes have been observed. At a critical coverage of half a monolayer, the oxide growth mode changes from two- to three-dimensional. At higher oxide coverages ($\Theta\geqslant2.0$ MLE) the surface is homogeneously covered by small 3D V_2O_3 crystallites. The morphology and the structure of the low-coverage 2D oxide phase has been observed to be strongly dependent on the oxide preparation conditions, such as ambient oxygen pressure and substrate temperature. The latter was found to control the balance of the adatom diffusion on the substrate terraces and along the edge boundaries of the growing oxide islands, which leads to different island growth processes. Under V-oxide evaporation conditions of $p(O_2)=2\times10^{-7}$ mbar, $T=523$ K, a porous fractal-type network is produced, which suggests a low edge mobility under these conditions. The STM images show, however, that the network is ordered at the atomic scale, exhibiting a $p(2\times2)$ honeycomb surface structure. Annealing of this phase in UHV to 623 K leads to the formation of more compact 2D oxide islands, which display the same $p(2\times2)$ structure in the atomically resolved STM images and in LEED. This ripening process is associated with the removal, presumably by subsurface migration, of surface oxygen, which may act as a diffusion inhibitor. At 673 K the V-oxide islands begin to decompose into V/Pd surface alloy and 2D metallic V islands. The V/Pd surface alloy shows ordered structure in the STM images with a strong bias dependence, displaying a hexagonal pattern at high positive bias and a wagon-wheel structure at low positive bias.

The *ab initio* total-energy DFT calculations have demonstrated that the $p(2\times2)$ honeycomb V-oxide structure can be described by a surface-V_2O_3 model, which is characterized by two vanadium atoms, occupying the fcc and hcp hollow sites on the Pd(111) surface, and three oxygen atoms adsorbed in the V-V bridge sites. This surface-V_2O_3 model is clearly distinguished from the bulk V_2O_3 structure. The simulated STM images based on this model agree very well with the experimentally observed honeycomb structure. Other structure models with different formal stoichiometries have been considered, but have been discarded on the basis of energetics and STM simulations. The surface-V_2O_3 structure exhibits a calculated initial state V $2p$ core-level shift of 1 eV with respect to the bulk V_2O_3 core-level binding energy, which is due to the direct contact of the V atoms with the Pd substrate in this model. This is consistent with the observed values in the XPS experiments.[8] Thus it appears that at low oxide coverages ($\leqslant0.5$ ML) a 2D surface-V_2O_3 layer is formed on Pd(111), which constitutes an interface-stabilized oxide phase. With increasing coverage, this surface phase eventually transforms into a V_2O_3 layer with bulk structural properties. This transformation of the surface-V_2O_3 layer into the bulk-type V_2O_3 phase and the associated intermediate structures will be the subject of a forthcoming paper.[9]

ACKNOWLEDGMENT

This work was supported by the Joint Research Program ''Gas-Surface Interactions'' of the Austrian Science Foundation.

[1] V. E. Henrich and P. A. Cox, *The Surface Science of Metal Oxides* (Cambridge University Press, Cambridge, 1993).
[2] B. Grzybowska-Swierkosz, Appl. Catal., A **157**, 1 (1997).
[3] K. B. Lewis, S. T. Oyama, and G. A. Somorjai, Surf. Sci. **233**, 75 (1990).
[4] K. Kishi, K. Hirai, and T. Yamamoto, Surf. Sci. **290**, 309 (1993).
[5] K. Kishi, Y. Hayakawa, and K. Fujiwara, Surf. Sci. **356**, 171 (1996).
[6] K. Kishi and K. Fujiwara, J. Electron Spectrosc. Relat. Phenom. **85**, 123 (1997).
[7] Th. Hartmann and H. Knözinger, Z. Phys. Chem. (Munich) **197**, 113 (1996).
[8] F. P. Leisenberger, S. Surnev, L. Vitali, M. G. Ramsey, and F. P. Netzer, J. Vac. Sci. Technol. A **17**, 1743 (1999).
[9] S. Surnev, G. Kresse, M. G. Ramsey, and F. P. Netzer (unpublished).
[10] J. Kraft, M. G. Ramsey, and F. P. Netzer, Phys. Rev. B **55**, 5384 (1997).
[11] W. Kohn and L. Sham, Phys. Rev. **140**, A1133 (1965).
[12] M. C. Payne, M. P. Teter, D. C. Allan, T. A. Arias, and J. D. Joannopoulos, Rev. Mod. Phys. **64**, 1045 (1992).
[13] G. Kresse and J. Hafner, Phys. Rev. B **48**, 13 115 (1993).
[14] G. Kresse and J. Furthmüller, Comput. Mater. Sci. **6**, 15 (1996); Phys. Rev. B **54**, 11 169 (1996).
[15] P. E. Blöchl, Phys. Rev. B **50**, 17 953 (1994).
[16] G. Kresse and D. Joubert, Phys. Rev. B **59**, 1758 (1998).

[17] G. Kresse, J. Hafner, S. Surnev, M. G. Ramsey, and F. P. Netzer (unpublished).
[18] J. P. Perdew, J. A. Chevary, S. H. Vosko, K. A. Jackson, M. R. Pederson, D. J. Singh, and C. Fiolhais, Phys. Rev. B **46**, 6671 (1992).
[19] H. J. Monkhorst and J. D. Pack, Phys. Rev. B **13**, 5188 (1972).
[20] M. Methfessel and A. T. Paxton, Phys. Rev. B **40**, 3616 (1989).
[21] W. Weiss and M. Ritter, Phys. Rev. B **59**, 5201 (1999).
[22] H. Hanneman, C. A. Ventrice, Jr., Th. Bertrams, A. Brodde, and H. Neddermeyer, Phys. Status Solidi A **146**, 289 (1994).
[23] H. C. Galloway, J. J. Benítez, and M. Salmeron, J. Vac. Sci. Technol. A **12**, 2302 (1994).
[24] Z. Zhang and M. G. Lagally, Science **276**, 377 (1997).
[25] H. Brune, Surf. Sci. Rep. **31**, 121 (1998).
[26] F. P. Leisenberger, M. Sock, G. Koller, S. Surnev, M. G. Ramsey, F. P. Netzer, B. Klötzer, and K. Hayek, Surf. Sci. **445**, 380 (2000).
[27] G. Kresse (unpublished).
[28] L. P. Zhang, J. van Ek, and U. Diebold, Phys. Rev. B **57**, R4285 (1998); **59**, 5837 (1999).
[29] M. Sock, G. Kresse, S. Surnev, M. G. Ramsey, and F. P. Netzer (unpublished).
[30] F. P. Leisenberger, S. Surnev, G. Koller, M. G. Ramsey, and F. P. Netzer, Surf. Sci. **444**, 211 (2000).